

---

# Studies of Small Biological Molecules

In this chapter, the interactions of small molecules with proteins are discussed in terms of different experimental methods with examples. The last section describes examples to study metabolic pathways using NMR experiments. Key questions to be answered include:

1. What are the experiments available to study the interactions of small molecules with proteins?
2. What kind of information can the experiments provide?
3. What types of systems are suitable for a particular experiment?
4. Can simple NMR experiments be used to study metabolic pathways?
5. What are the advantages of NMR experiments compared to other techniques in such research?

## 6.1. LIGAND–PROTEIN COMPLEXES

As NMR spectroscopy has been widely used to determine the structures and dynamics of molecules ranging from synthetic compounds to macro biomolecules, it has become a powerful approach for studying the interactions between proteins (and/or nucleic acids) and ligands. The interactions can be studied by observing a change in NMR phenomena (signal) that is induced by the binding. For this purpose, a variety of pulse sequences has been implemented to observe changes in chemical shifts, mobility, relaxation properties, and NOEs, etc. Some of the methods make full use of the difference in mass between protein and ligands, such as methods measuring the diffusion and relaxation of ligands, whereas others observe binding-induced changes such as chemical shifts, NOE, and  $^1\text{H}$  exchange rate.

### 6.1.1. SAR-by-NMR Method

SAR by NMR (Structure–Activity Relationship) measures the chemical shift changes of  $^1\text{H}$  and  $^{15}\text{N}$  spins at binding sites of target proteins upon the binding of small molecule ligands. The binding affinity of ligands can be improved by directly linking together two weak binding ligands to obtain a high affinity binding ligand. The SAR-by-NMR method can also be used to locate binding sites on the target protein (Shuker *et al.*, 1996).

The main point of SAR-by-NMR can be understood by looking at the dissociation constants of the complexes. For each binding site, an equilibrium is established by three species: the target protein, ligand, and the complex. For a binding equilibrium:



the dissociation constant  $K_D$  is given by  $\Delta G$ :

$$RT \ln(K_D) = \Delta G \quad (6.2)$$

in which  $R$  is the ideal gas constant,  $T$  is the absolute temperature, and  $\Delta G$  is the free energy difference. For the individual binding sites A and B, the dissociation constants  $K_D^A$  and  $K_D^B$  are given by:

$$RT \ln(K_D^A) = \Delta G^A \quad \text{and} \quad RT \ln(K_D^B) = \Delta G^B \quad (6.3)$$

When a single ligand occupies two sites simultaneously,



in which P, L, and C stand for protein, ligand, and complex, respectively. Then

$$\begin{aligned} RT \ln(K_D^{AB}) &= \Delta G^{AB} \\ &= RT \ln(K_D^A) + RT \ln(K_D^B) \end{aligned} \quad (6.5)$$

$$\Delta G^{AB} = \Delta G^A + \Delta G^B \quad (6.6)$$

Therefore,  $K_D^{AB} = K_D^A * K_D^B$ . If the binding dissociation constant  $K_D^A$  is  $3 \times 10^{-4}$  and  $K_D^B$   $1 \times 10^{-3}$ , the dissociation constant  $K_D^{AB}$  of the structurally linked ligand is close to  $3 \times 10^{-7}$ , which is much lower than that for each of the individual ligands.

The dissociation constant  $K_D$  can be estimated from the observed chemical shift changes in the complex. For a single-site binding,  $K_D$  is given by:

$$K_D = \frac{[L][P]}{[C]} \quad (6.7)$$

in which  $[L]$ ,  $[P]$ , and  $[C]$  are the equilibrium concentrations of the free ligand, free protein, and the complex, respectively. Assuming that the complex is formed by a 1 : 1 ratio and the ligand concentration  $[L]_0$  is in high excess to that of the protein  $[P]_0$ , the equilibrium concentrations can be expressed by:

$$[C] = \frac{\delta - \delta_f}{\delta_s - \delta_f} [P]_0 \quad (6.8)$$

$$[L] = [L]_0 - [C] \quad (6.9)$$

$$[P] = [P]_0 - [C] \quad (6.10)$$

in which  $\delta$  and  $\delta_f$  are the chemical shifts in the presence and absence of ligand, respectively, and  $\delta_s$  is the chemical shift at saturation level of the ligand, that is, the target protein is completely bound. Therefore,  $K_D$  can be estimated according to:

$$K_D = \frac{([L]_0 - [C])([P]_0 - [C])}{[C]} \quad (6.11)$$

In some situations, the affinity of the binding ligand is described in terms of its concentration  $IC_{50}$  which is the concentration of the inhibitor (or ligand) required for 50% inhibition (or binding) of the target protein. The  $K_D$  of a ligand with an  $IC_{50}$  can also be derived from the known dissociation constant  $K_I$  of the inhibitor for a given concentration  $[I]$  of the inhibitor:

$$K_D = \frac{IC_{50} K_I}{[I]} \quad (6.12)$$

The equation is obtained using the previously stated assumptions and  $[I]$  is much higher than  $K_I$  (Cheng and Prusoff, 1973).

A  $^1H$ - $^{15}N$  HSQC experiment is utilized to observe the changes in chemical shifts of an  $^{15}N$  labeled target protein with and without small molecules. The  $^1H$  chemical shifts of an unlabeled small molecule will not interfere with the observed signals of the protein because only  $^1H$ - $^{15}N$  correlations can be observed. The binding of the ligand to the protein is determined by comparing the HSQC spectrum of the target protein along with the one in the presence of the small molecule. If there are significant cross-peak shifts in the mixture compared to the free protein, the small molecule compound is determined to bind to the protein and is considered a lead compound. A library of small molecule compounds is used for the screening. Once a weak binding lead compound is identified based on the chemical shift change, the value of the dissociation constant  $K_D$  is determined. The binding affinity to this site is optimized using a derivative analog of the lead compound, which leads to a relatively strong-binding ligand. The binding of a new ligand on a second site is located by observing, in the presence of the optimized ligand, the chemical shift changes of a different set of amide  $^1H$ - $^{15}N$  cross-peaks that come from different residues than the first site. Then, the second ligand is optimized in the same way as the first one. The two ligands are structurally linked together to form the final ligand that binds to the two sites of the protein simultaneously (Figure 6.1). The location of the linkage and the stereo orientation of the two ligands play an important role in obtaining a high-affinity ligand, and are determined based on the information of protein structure as well as the information on the binding geometry of the two individual ligands with respect to the protein.

High-affinity ligands binding to a number of proteins have been discovered utilizing the SAR-by-NMR method (Shuker *et al.*, 1996; Hajduk *et al.*, 1997b). For instance, the method has been utilized to identify new ligands for leukocyte function-associated antigen-1 (LFA-1), that is a cell surface adhesion receptor involved in the inflammatory and certain T-cell immune responses (Gahmberg, 1997) when complexed with intracellular adhesion molecules (ICAM-1). Inhibitors to the interaction between LFA-1 and ICAM-1 may have therapeutic uses in treating inflammatory diseases (Sligh *et al.*, 1993). Although certain compounds have been identified to prevent the binding of ICAM-1 to LFA-1, poor solubility and side effects make them undesirable (Liu *et al.*, 2000). The NMR method was used to screen for new compounds with improved pharmaceutical properties. Compound A (Figure 6.2) was identified to bind to LFA-1 with a  $K_D$  of approximately 1 mM by observing the chemical shift changes of amide

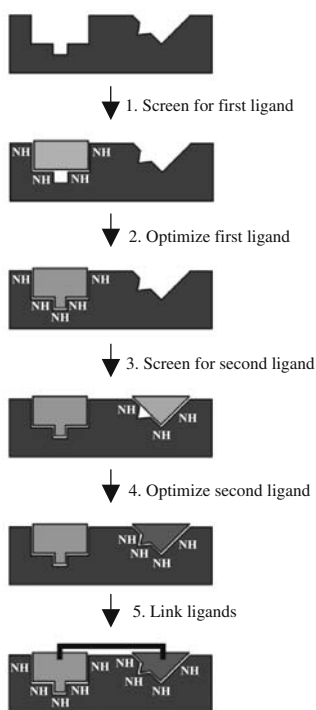


**Figure 6.1.** Drug screening by the SAR-by-NMR method (reproduced with permission from Shuker *et al.*, *Science* 274, 1531, 1996. Copyright © 1996 AAAS).

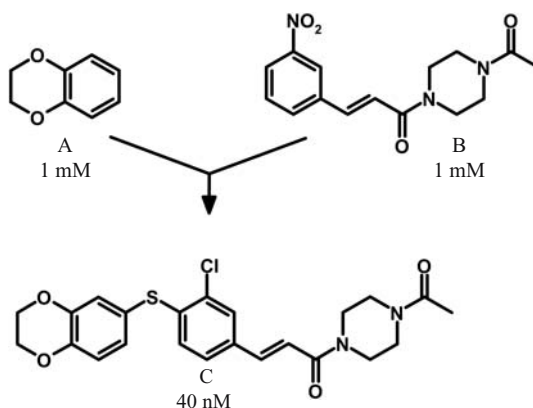


**Figure 6.2.** Constructing the ligand for leukocyte function-associated antigen-1 (LFA-1) utilizing the SAR-by-NMR method. Compound A was identified first by NMR screening, and was used at a saturating concentration to identify compound B binding to a different region of the protein. Based on the structural information of the two compounds and the target protein, compound C was synthesized and binds to the target protein with improved affinity and other pharmaceutical properties.

$^1\text{H}$  and  $^{15}\text{N}$  in an HSQC spectrum. Subsequently, the second ligand (compound B) was found to bind a different region of LFA-1 in the presence of compound A at a saturating concentration with a similar  $K_D$  value. Based on the structural information of the two ligands and LFA-1, a number of compounds were synthesized, of which compound C has an  $\text{IC}_{50}$  value of 40 nM with increased solubility (Liu *et al.*, 2001).

### 6.1.2. Diffusion Method

While SAR-by-NMR measures the change in chemical shifts of the target protein, the diffusion method makes use of the change in the translational diffusion rate of a ligand upon binding to the target protein. Because the observed signals are from the ligand, it is not necessary to use an isotope labeled protein. The translational diffusion coefficient  $D$  for a spherical molecule with radius  $r$  in a solvent of viscosity  $\eta$  has a dependence of  $1/r$ , according to the Stokes–Einstein equation (Stilbs, 1987):

$$D = \frac{KT}{6\pi\eta r} \quad (6.13)$$

in which  $K$  is the Boltzmann constant and  $T$  is the absolute temperature. Therefore, the  $D$  of a ligand has a smaller value when a complex is formed by the ligand with a protein.

There are many versions of NMR experiments available to measure the diffusion coefficient, based on the pioneering work by Stejskal and Tanner using pulse field gradient NMR methods (Stejskal and Tanner, 1965; Johnson Jr., 1999). The LED sequence (longitudinal eddy-current delay) was proposed to reduce artifacts caused by eddy-currents as well as to avoid extensive loss from  $T_2$  relaxation by placing the magnetization along the  $z$ -axis for most of the experiment time. The signal intensities of a ligand are attenuated in a series of spectra as a function of the strength  $G$  and duration  $\tau$  of a rectangular gradient and the diffusion time  $\Delta$  between the two gradient echo pulses (Figure 6.3) according to Price and Kuchel (1991):

$$\ln \frac{I(G)}{I(0)} = -(\gamma\tau G)^2 \left( \Delta - \frac{\tau}{3} \right) D \quad (6.14)$$

in which  $I(G)$  and  $I(0)$  are the signal intensities observed with and without gradient  $G$ , respectively, and  $\gamma$  is the proton gyromagnetic ratio. The signal attenuation for large molecules requires increasing the amplitude of the quantity  $(\gamma\delta G)^2(\Delta - \tau/3)$ . The value of  $D$  is obtained from the slope by plotting  $I(G)/I(0)$  vs  $G^2$ . For large proteins, diffusion coefficients are on the

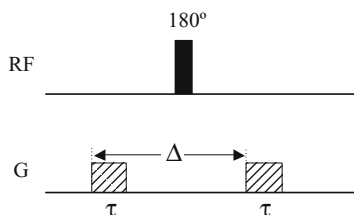


**Figure 6.3.** Gradient spin echo sequence for measuring the diffusion constant.

order of  $10^{-6} \text{ cm}^2 \text{ s}^{-1}$ , whereas small molecules have diffusion coefficients of  $c. 10^{-5} \text{ cm}^2 \text{ s}^{-1}$ . For example, a lysozyme, a globular protein of 14.5 kDa, has a  $D$  value of  $1.06 \times 10^{-6} \text{ cm}^2/\text{s}^{-1}$  and hemoglobin, a protein of  $c. 65 \text{ kDa}$ , has a diffusion coefficient of  $0.69 \times 10^{-6} \text{ cm}^2 \text{ s}^{-1}$  compared to sucrose and alanine which have  $D$  values of  $0.52 \times 10^{-5} \text{ cm}^2 \text{ s}^{-1}$  and  $0.86 \times 10^{-5} \text{ cm}^2 \text{ s}^{-1}$ , respectively (Stilbs, 1987; Dalvit and Böhlen, 1997). The delay  $\Delta$  is typically set up in the range of 100–500 ms, whereas the delay  $\delta$  is selected within several milliseconds. The spectra are obtained with variable gradient strengths, usually less than  $10 \text{ G cm}^{-1}$  for small free ligands and up to  $50 \text{ G cm}^{-1}$  for ligands bound to proteins.

Although the diffusion coefficient can be determined by the LED sequence with acceptable accuracy, a qualitative analysis of the diffusion behaviors of free and bound ligands provides useful information for studying protein–ligand binding. Two spectra are acquired for the ligand sample in the presence and absence of the protein. Because the translational motion of a bound ligand will be slower than that of a free ligand, the gradient strength required to decrease the signals of ligands in a mixture with protein is higher if the ligand forms a complex with the protein than if the ligand stays free in solution. For example, if a free ligand has a diffusion constant of  $c. \text{ five times larger than the protein}$ , the gradient strength,  $G_f$ , used to reduce the signal intensity of the free ligand is half the value of gradient,  $G_b$ , needed to decrease the intensity of the bound ligand by the same amount:

$$G_f = \frac{G_b}{\sqrt{5}} \approx \frac{G_b}{2} \quad (6.15)$$

or the intensity of the bound ligand will be higher than the non-bound one at the same gradient strength:

$$I_f/I_0 = (I_b/I_0)^{5 \times 2.303} \approx (I_b/I_0)^{11.5} \quad (6.16)$$

Since  $I_b/I_0$  is always less than one, the intensity of the free ligand is much smaller than the complexed ligand when applying the same gradient strength. Therefore, the bound state can be recognized by comparing the intensity change of the two sets of spectra acquired by arraying the gradient in the same steps. The observable change in the diffusion property of a ligand is dependent on both the diffusion coefficient and the concentration of bound ligand,  $[C]$ . If  $[C]$  is low due to a low concentration of protein, the change caused by the binding may be too small to be observed. To prevent the binding-induced diffusion change from being below the detection limit, the concentration of ligand should not exceed twice that of the protein. Figure 6.4 shows an example of using the diffusion experiments to identify ligands.

### 6.1.3. Transferred NOE

The cross-relaxation rate  $\sigma$  is dependent on the distance between the two spins and the rotational correlation time. For large molecules such as proteins with a large correlation time  $\tau_c$ , the cross-relaxation rate has an opposite sign to that of small molecules and the rate is significantly higher in magnitude than the small molecules. In bound state, the ligand will have a correlation time determined by the protein of the complex. Therefore, a ligand exchanging between the bound and unbound states will have alternating cross-relaxation rates with opposite signs and different magnitudes. When the chemical exchange of a ligand between equilibrated

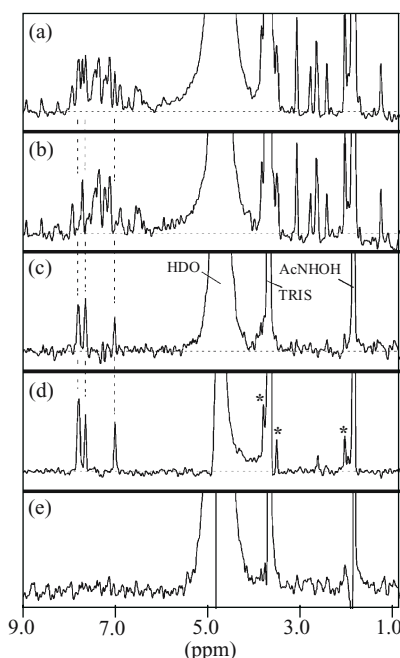


**Figure 6.4.** Identification of 4-cyano-4'-hydroxybiphenyl as a ligand for stromelysin from a mixture containing eight other non-binding compounds using diffusion editing. (a) Diffusion-edited  $^1\text{H}$  NMR spectrum of the nine compounds in the absence of stromelysin recorded with low gradient strength. (b) Diffusion-edited  $^1\text{H}$  NMR spectrum of the nine compounds in the presence of stromelysin recorded with low gradient strength after subtracting a similar spectrum recorded with high gradient strength (to remove the protein signals). (c) Difference spectrum of (a) minus (b), which shows the resonances of the bound ligand. (d) Reference spectrum of the ligand. (e) Difference spectrum similar to spectrum (c) recorded on solutions containing only the eight non-binding compounds. The dashed lines in (c) and (d) correspond to the ligand resonances. Buffer impurities are denoted with asterisks (reproduced with permission from Hajduk *et al.*, *J. Am. Chem. Soc.* 119, 12257, 1997. Copyright © 1997 American Chemical Society).

free and bound states is much faster than the cross-relaxation rate, the change in magnetization arising from the NOE between the protein and bound ligand protons is transferred to the proton spins of the free ligand. Therefore, for small ligands, the cross-relaxation rate and hence the observed NOE changes sign upon binding to proteins. This transferred NOE has been used to characterize the binding of ligands to proteins (Clore and Gronenborn, 1982; Ni, 1994).

NOESY and ROESY experiments are used to observe the transferred NOE cross-peaks of the ligand. The observed NOE of a ligand in a NOESY will change sign upon the formation of a protein–ligand complex. Since both intermolecular (between ligand and protein) and intramolecular NOEs are observed simultaneously, the opposite sign of the cross-peaks of the free ligand may scale down the intensities of bound ligand in NOESY spectra. A standard NOESY pulse sequence can be utilized with minor modifications to remove the protein resonances. The crucial modification is to insert a relaxation filter sequence, such as a spin echo in the relaxation period or sometimes at the end of the NOESY sequence. When using the spin echo at the end of NOESY, it also serves the purpose to obtain solvent suppression by suppressing both the protein resonances and the water signal simultaneously.

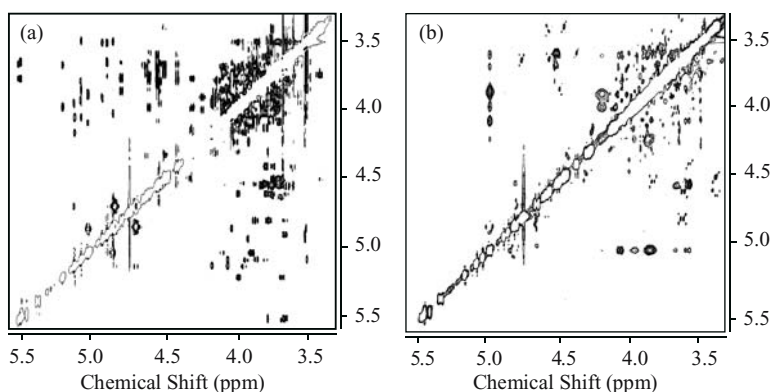


**Figure 6.5.** 2D  $^1\text{H}$  NOESY spectra of a 15-member oligosaccharide library in the (a) absence and (b) presence of agglutinin. Observed NOEs are positive in (a) and negative in (b). In (b), a spin-lock filter was used to remove protein resonances, and transfer NOE correlations are observed only for the oligosaccharide  $\alpha\text{-L-Fuc-(1}\rightarrow\text{6)-}\beta\text{-D-GlcNAc-OMe}$  (reproduced with permission from Meyer *et al.*, *Eur. J. Biochem.* 246, 705, 1997. Copyright © 1997 Blackwell Publishing).

An alternative way to suppress the protein resonances is to place two orthogonal composite-pulse spin lock trains (e.g., DIPSI-2) at the beginning of the relaxation period of the NOESY sequence. However, the composite-pulse spin lock sequence requires a longer relaxation filtering time owing to the fact that the effective relaxation during the composite pulses is determined by the trajectory average of the  $T_1$  and  $T_2$  relaxation rates. Figure 6.5 shows the application of a transferred NOESY experiment in identifying the ligand binding to agglutinin from a mixture of small compounds (Meyer *et al.*, 1997). For the mixture sample in the absence of agglutinin (Figure 6.5a), the compounds give rise to NOE cross-peaks with positive intensities. In the presence of the protein, the cross-peaks of the compounds retain the same sign as the diagonal peaks, except for one ligand showing transferred NOE correlations observed with negative intensities (Figure 6.5b).

#### 6.1.4. Saturation Transfer Difference

For large proteins, a cross-relaxation directly proportional to the correlation time  $\tau_c$  dominates the relaxation process, causing extremely rapid magnetization transfer throughout the protein. Selective saturation of any protein resonances results in saturation of all protein protons as a consequence of the rapid magnetization transfer via the efficient cross-relaxation within the protein. Therefore, saturation can be achieved by a long irradiation on any resonance of the protein (i.e., any spectral region) in the 1D NOE difference experiment (Klein *et al.*, 1999; Mayer and Meyer, 1999).

In practice, a spectral region away from ligand resonances is selected for the saturation, typically the upfield aliphatic resonances. The 1D saturation transfer difference (STD) experiment subtracts the spectrum observed by the selective saturation of protein resonances with the one recorded by selectively saturating an off-resonance region away from protein and ligand resonances. The subtraction is normally achieved during the experiment by inverting the receiver phase for alternating on- and off-resonance acquisitions to avoid the introduction of artifacts induced by the subtraction.



When a ligand binds to a protein, the saturation of the protein resonances will also saturate ligand resonances owing to cross-relaxation. The 1D STD method consists of two experiments collected with interleaved acquisition. The first experiment is collected with on-resonance irradiation selective at an aliphatic resonance of the protein. The intensity of the bound ligand will decrease as a consequence of the saturation transfer via cross relaxation. The second experiment is carried out with the irradiation selected at an off-resonance empty region with inverted receiver phase. In this experiment, resonances of neither the protein nor ligand are saturated, hence, no saturation transfer occurs. Subsequently, the two data sets are added and stored (the net effect is subtraction of the data because of inversion in the receiver phase for the off-resonance experiment). The difference spectrum contains only signals of the ligand bound to protein, whose intensity is decreased by the saturation.

As in the NOE-based experiment, a  $T_2$  relaxation filter can be inserted into the 1D STD pulse sequence to suppress the unwanted resonances from the protein. Hahn spin echo and spin lock sequences yield superior suppression of signals arising from protein. The STD experiment is a significantly sensitive method since a large ratio of ligand to protein can be used to observe the saturation transfer.

Figure 6.6 illustrates an example for the application of the STD method for studying the binding of RCA120 lectin protein to a ligand (Mayer and Meyer, 2001). The peaks from the ligand binding to the protein appear in the STD spectrum. It is demonstrated that the background signals from protein resonances have been significantly suppressed in the STD (Figure 6.6f) and protein reference (c) spectra recorded with the spin

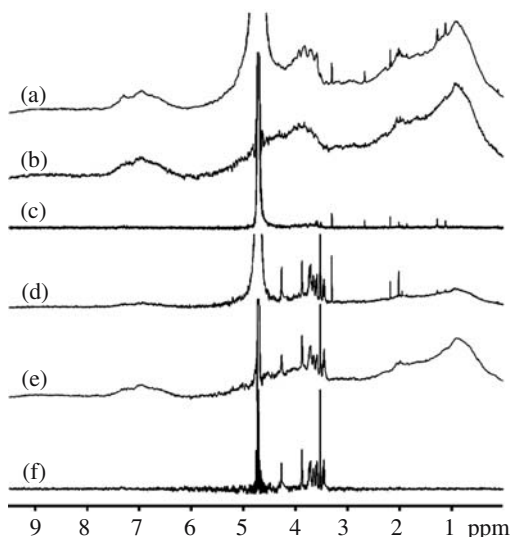


**Figure 6.6.** STD  $^1\text{H}$  experiments to study the binding of methyl  $\beta$ -D-galactopyranoside as a ligand to the RCA120 lectin. (a) Reference spectrum of RCA120 lectin. (b) STD spectrum of RCA120 lectin. (c) Reference spectrum of RCA120 lectin recorded with a spin-lock filter. (d) Reference spectrum of RCA120 lectin in the presence of a 30-fold excess of methyl  $\beta$ -D-galactopyranoside. (e) STD spectrum of RCA120 lectin plus methyl  $\beta$ -D-galactopyranoside. (f) STD spectrum as in (e) but with the addition of a spin-lock filter (reproduced with permission from Mayer and Meyer, *J. Am. Chem. Soc.* 123, 6108, 2001. Copyright © 2001 American Chemical Society).

lock transverse relaxation filter, compared to the one acquired using the standard STD sequence (e).

### 6.1.5. Isotope-Editing Spectroscopy

Isotope enrichment has made it possible to observe different partners of a complex individually in a way such that only the magnetization originating from the desired part of the complex and then transferred to the other part of the complex via cross-relaxation is observed. Either the ligand or protein can be isotope labeled with  $^{15}\text{N}$ ,  $^{13}\text{C}$ , and/or  $^2\text{H}$ . Isotope-edited (also known as isotope-selected) experiments can be used to study a ligand/protein complex with isotope enriched ligand. For ligands labeled with  $^{13}\text{C}$ , the 2D version of the 3D NOESY- $^1\text{H}$ ,  $^{13}\text{C}$ -HMQC experiment (Figure 6.7a) can be applied to observe the intermolecular NOE

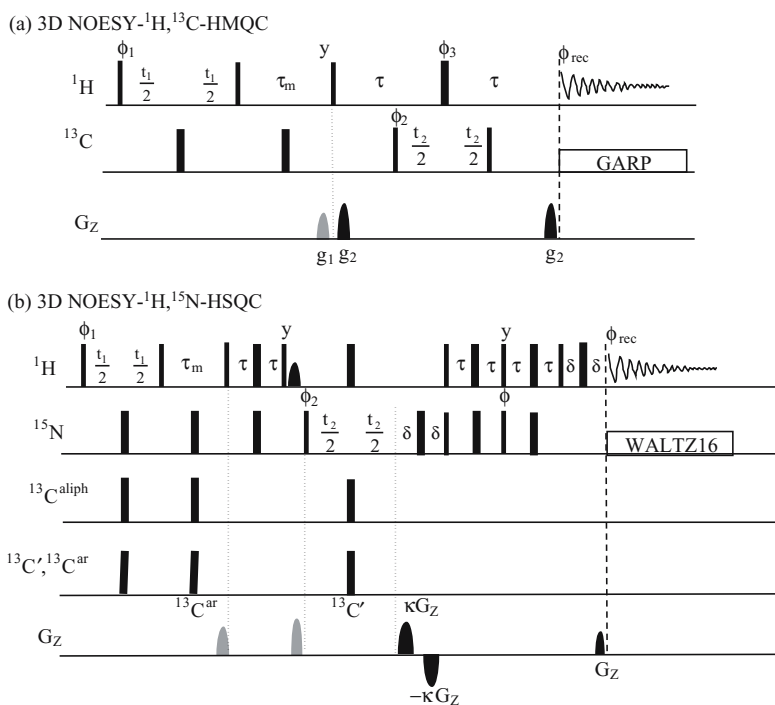


**Figure 6.7.** Pulse sequences for 3D  $^{13}\text{C}$ -edited NOESY (NOESY- $^1\text{H}$ ,  $^{13}\text{C}$ -HMQC) and 3D  $^{13}\text{C}$ -edited NOESY (NOESY- $^1\text{H}$ ,  $^{15}\text{N}$ -HSQC) experiments. (a) In the 3D  $^{13}\text{C}$ -edited NOESY, all pulses are  $x$  phased, except that  $\phi_1 = x, -x, +\text{States-TPPI}$  ( $t_1$ ),  $\phi_2 = x, x, -x, -x + \text{States-TPPI}$  ( $t_2$ ), and  $\phi_{\text{rec}} = x, -x, -x, x$ . The delay  $\tau = 3.8$  ms. The shaded gradient is used to destroy the residual transverse magnetization due to the imperfect  $180^\circ$  pulses;  $G_z$  gradients for coherence selection. (b) In the 3D  $^{15}\text{N}$ -edited NOESY experiment with sensitivity enhancement, the delay  $\tau = 2.7$  ms,  $\delta$  equals the  $G_z$  gradient pulse length. All pulses are  $x$  phased, except that  $\phi_1 = 45^\circ, 225^\circ + \text{States-TPPI}$  ( $t_1$ ),  $\phi_2 = x, x, -x, -x, +\text{States-TPPI}$  ( $t_2$ ), and  $\phi_{\text{rec}} = x, -x, -x, x$ . For PEP sensitivity enhancement,  $k = \pm 10$ ,  $\phi = \pm y$ .

cross-peaks of  $^{13}\text{C}$ -labeled ligand to the complexed protein and  $^1\text{H}$  signals from unlabeled protein are not observable. As a result, these cross-peaks are readily identified due to the fact that they only appear on one side of the diagonal. The delay between the two  $^{13}\text{C}$   $90^\circ$  pulses (where the  $t_2$  evolution was in the 3D sequence) is set as short as possible. The sample of the labeled ligand with unlabeled protein is usually dissolved in  $^2\text{H}_2\text{O}$  solution. Thus, the HMQC block in the sequence provides sufficient suppression of residual water in  $^2\text{H}_2\text{O}$ .

Although this experiment provides a convenient and reliable means to determine the binding of the complex, isotope-labeling synthetic compounds requires tremendous efforts, if it is even possible. However, isotope-labeled peptides serving as ligands are commercially available and are easier to prepare. For a protein–peptide complex,  $^{15}\text{N}$ -edited 2D or 3D NOESY experiments can also be applied to obtain information on the binding site. The PEP sensitivity-enhanced version of the 3D NOESY- $^1\text{H}$ ,  $^{15}\text{N}$ -HSQC pulse sequence shown in Figure 6.7b utilizes a gradient echo to select the heteronuclear  $^{15}\text{N}$  coherence of the peptide whose amide protons have NOEs to the bound protein. For a large peptide, it is necessary to introduce the heteronuclear frequency dimension in order to overcome difficulty in extracting the NOE intensity caused by the overlap of cross-peaks. Resolving the NOESY cross-peaks into the additional heteronuclear dimension significantly improves the resolution.

Shown in Figure 6.8 is an example of the application of the  $^{13}\text{C}$  edited NOESY experiment to study the complex formed by unlabeled cyclophilin with cyclosporin A (ligand) uniformly  $^{13}\text{C}$ -labeled at MeLeu<sup>9</sup> and MeLeu<sup>10</sup> (Fesik *et al.*, 1990). In the  $\omega_1$  ( $F_1$ ) dimension, only  $^{13}\text{C}$  attached protons of the ligand are observed. In the  $\omega_2$  ( $F_2$ ) dimension, the NOE cross-peaks between the ligand and the protein are observed. Since the cross-peaks of protein–ligand only appear in the  $\omega_2$  dimension, they are readily identified by comparing both dimensions.

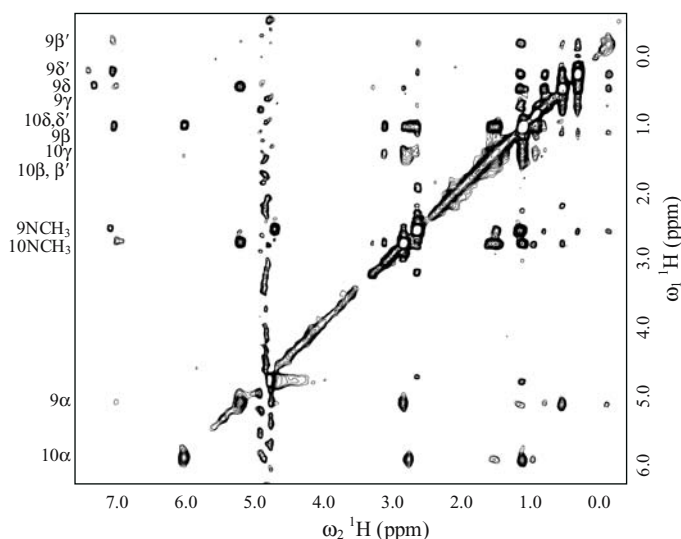


**Figure 6.8.**  $^{13}\text{C}$ -isotope edited NOESY spectrum of  $[\text{U-}^{13}\text{C-MeLeu}^{9,10}]$ CsA bound to human cyclophilin. Assignments for the MeLeu<sup>9</sup> and MeLeu<sup>10</sup> protons of CsA are given at the left of the spectrum (reproduced with permission from Fesik *et al.*, *Science* 250, 1406, 1990. Copyright © 1990 AAAS).

### 6.1.6. Isotope-Filtering Spectroscopy

When isotope-labeled protein is available, structural information on the protein–ligand complex can be obtained by an  $^{15}\text{N}$ ,  $^{13}\text{C}$  isotope-filtered experiment, in which only the intermolecular NOEs of the unlabeled ligand with the labeled protein are observed by suppressing the intramolecular NOEs among the protein resonances. The term “ $^{13}\text{C}$ -filtered” means that the signals from the  $^{13}\text{C}$ -attached protons are suppressed in the experiment, whereas “ $^{13}\text{C}$ -edited” or “ $^{13}\text{C}$ -selected” denotes that the signals from the  $^{13}\text{C}$ -attached protons are selected in the experiment (Breeze, 2000). The application of the heteronuclear filter on one dimension of the 2D experiment is also called half X-filter and, thus, a 2D NOESY- $^1\text{H}$ ,  $^{13}\text{C}$ -HMQC pulse sequence may be termed as a  $^{13}\text{C}$ -half-filtered ( $\omega_1$ ) NOESY if the filter is on the  $t_1$  dimension, or as a  $^{13}\text{C}$ -half-filtered ( $\omega_2$ ) NOESY if the filter is on the  $t_2$  dimension. Alternatively, the X-filtering can also be applied to both dimensions. However, additional half X-filtering will lengthen the pulse sequence, which makes the experiment less sensitive due to relaxation effects.

Because of a wide range of  $^1\text{H}$ – $^{13}\text{C}$  couplings, a  $^{13}\text{C}$  half-filtered experiment cannot completely filter out the magnetization of protons directly bound to the heteronucleus. As a consequence, the spectrum contains residual signals from the labeled proteins. To minimize the residual magnetization of the labeled protein, several heteronuclear filtering building blocks have been utilized. The double isotope-filter (also known as a double-tuned filter) is a sequential combination of two single filters, shown in Figure 6.9a (Gemmecker *et al.*, 1992). The delays in the two filters are selected for different couplings. At the end of the first isotope-filter, the anti-phase sine component after the echo is transformed by a  $90^\circ$   $S$  pulse to double-quantum coherence  $2I_x S_y$  which cannot be transformed into observable magnetization throughout the rest of the pulse sequence:

$$\begin{aligned} \text{Spin } I-S : \quad -I_y &\xrightarrow{\tau' \rightarrow \pi(I_x + S_x) \rightarrow \tau'} -I_y \cos(\pi J_{IS} 2\tau') - 2I_x S_z \sin(\pi J_{IS} 2\tau') \\ &\xrightarrow{\frac{\pi}{2} S_x} -I_y \cos(\pi J_{IS} 2\tau') + 2I_x S_y \sin(\pi J_{IS} 2\tau') \end{aligned} \quad (6.17)$$

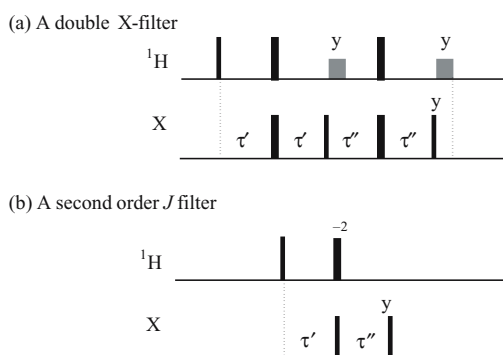


**Figure 6.9.** Isotopic filter schemes for suppressing the signals of the heteronucleus-attached protons. All pulses are  $x$  phased except as indicated. The shaded pulses are spin-lock pulses. (a) A double isotope filter (or double-tuned filter) uses two consecutive X-half filters with different delays. The magnetization is suppressed by a factor of  $\cos(2\pi J_{IS} \tau') \cos(2\pi J_{IS} \tau'')$ . (b) A second order J filter uses two different delays that can be optimized for different values of the heteronuclear couplings, which provides a suppression by a factor of  $\cos(\pi J_{IS} \tau') \cos(\pi J_{IS} \tau'')$ . Both filters can be implemented in 2D or 3D pulse sequences.

After the second echo, the anti-phase sine component ( $-2I_x S_y$ ) is transformed by the  $S 90^\circ_y$  pulse into unobservable zero-quantum coherence  $2I_x S_x$ :

$$\begin{aligned} \xrightarrow{\tau'' \rightarrow \pi(I_x + S_x) \rightarrow \tau''} & -I_y \cos(\pi J_{IS} 2\tau') \cos(\pi J_{IS} 2\tau'') - 2I_x S_z \cos(\pi J_{IS} 2\tau') \sin(\pi J_{IS} 2\tau'') \\ \xrightarrow{\frac{\pi}{2} S_y} & -I_y \cos(\pi J_{IS} 2\tau') \cos(\pi J_{IS} 2\tau'') - 2I_x S_x \cos(\pi J_{IS} 2\tau') \sin(\pi J_{IS} 2\tau'') \quad (6.18) \end{aligned}$$

Therefore, the undesired magnetization of the labeled protein is scaled according to the factor of  $\cos(\pi J_{IS} 2\tau') \cos(\pi J_{IS} 2\tau'')$ . The magnetization of the uncoupled protons is not changed by the end of the double filtering:

$$\begin{aligned} -I_y & \xrightarrow{\tau' \rightarrow \pi(I_x + S_x) \rightarrow \tau' \rightarrow \frac{\pi}{2} S_x} -I_y \\ & \xrightarrow{\tau'' \rightarrow \pi(I_x + S_x) \rightarrow \tau'' \rightarrow \frac{\pi}{2} S_y} -I_y \quad (6.19) \end{aligned}$$

The two delays are set to  $1/(4J_{IS})$ , typically to 2.0 and 1.785 ms, to optimize the  $^1\text{CH}$  couplings of 125 Hz and 140 Hz, respectively, which yields excellent suppression for aliphatic  $^1\text{H}$ – $^{13}\text{C}$  signals, but moderate reduction of aromatic magnetization. Application of a spin-lock pulse on the  $y$ -axis with different lengths (1.0–2.0 ms) after each filter suppresses the anti-phase coherence and, thus, improves the suppression of the unwanted heteronucleus-coupled magnetization.

Another example sequence for suppressing the magnetization of a heteronucleus-attached proton is shown in Figure 6.9b. A “second order J filter” sequence uses two different delays that can be optimized for different values of the heteronuclear couplings, which provides efficient suppression of the heteronuclear coherence. The final magnetization of the heteronuclear magnetization at the end of the building block is scaled by a product of two coefficients as described in the double filtering scheme (Figure 6.9a). The heteronuclear coupled and uncoupled magnetization can be understood by the product operator. After the mixing period of the NOESY, the magnetization transfers for uncoupled and coupled spin  $I$  are given by:

$$\text{Spin } I: \quad -I_y \xrightarrow{\tau'} -I_y \xrightarrow{\pi I_x + \frac{\pi}{2} S_x} I_y \xrightarrow{\tau''} I_y \xrightarrow{\frac{\pi}{2} S_y} I_y \quad (6.20)$$

Because the delays  $\tau'$  and  $\tau''$  are short compared to the chemical shift, the magnetization of the uncoupled  $I$  spin is almost unchanged after the evolutions of  $\tau'$  and  $\tau''$ , whereas the coupled spin  $I$  undergoes the following coherence transfer precesses:

$$\begin{aligned} \text{Spin } I-S: \quad & -I_y \xrightarrow{\tau'} -I_y \cos(\pi J_{IS} \tau') + 2I_x S_z \sin(\pi J_{IS} \tau') \\ & \xrightarrow{\pi I_x + \frac{\pi}{2} S_x} I_y \cos(\pi J_{IS} \tau') - 2I_x S_y \sin(\pi J_{IS} \tau')_y \quad (6.21) \\ & \xrightarrow{\tau''} I_y \cos(\pi J_{IS} \tau') \cos(\pi J_{IS} \tau'') - 2I_x S_z \cos(\pi J_{IS} \tau') \sin(\pi J_{IS} \tau'') \\ & \xrightarrow{\frac{\pi}{2} S_y} I_y \cos(\pi J_{IS} \tau') \cos(\pi J_{IS} \tau'') - 2I_x S_x \cos(\pi J_{IS} \tau') \sin(\pi J_{IS} \tau'') \quad (6.22) \end{aligned}$$

The anti-phase sine component  $2I_x S_z$  after the  $\tau'$  and  $\tau''$  periods is converted into double- and zero-quantum coherence by the  $S$ - $90^\circ$  pulses, and are not transferred into observable

coherence throughout the isotope-filtered experiment. Therefore, at the end of the sequence the proton magnetization is unchanged, whereas the heteronuclear coherence is attenuated by the coefficient product:

$$\cos(\pi J_{IS}\tau') \cos(\pi J_{IS}\tau'') \quad (6.23)$$

The two delays are set to  $1/2J_{IS}$ . Recently, a filtering method using adiabatic inversion pulses (WURST pulses, see Adiabatic Pulses in Chapter 4) has been demonstrated to provide more efficient suppression of the heteronuclear coupling with variable sizes (Zwahlen *et al.*, 1997).

## 6.2. STUDY OF METABOLIC PATHWAYS BY NMR

The study of metabolic pathways in biological systems has been given new direction by recent application of NMR spectroscopy. Traditionally,  $^{14}\text{C}$  carbon tracers have extensively been used for these studies. However,  $^{14}\text{C}$  tracers have many practical disadvantages due to the radiation precautions and laborious sample handling that limit their applications for studies of the pathways in animals and humans. The use of  $^1\text{H}$  and  $^{13}\text{C}$  NMR to study the metabolic pathways by tracking the  $^{13}\text{C}$  enriched metabolic substances provides significant insight into how different metabolic processes are regulated *in vitro* and *in vivo*. Metabolic pathways are a series of consecutive chemical reactions to degrade specific simple molecules such as acetate and glucose and produce specific complex molecules in cells. Their reactants, intermediates, and products are referred to as metabolites. Each reaction is catalyzed by a distinct enzyme produced by the expression of a gene. Simple 1D  $^1\text{H}$  and  $^{13}\text{C}$  NMR experiments in combination with a  $^{13}\text{C}$  isotope labeling approach provide a means of studying the metabolites of specific pathways.

The first example is chosen from the study of the initial steps of the common aromatic amino acid pathway in *Methanococcus maripaludis* (Tumbula *et al.*, 1997). The pentose phosphate pathway produces pentoses for nucleosides and erythrose 4-phosphate (E4P) for the biosynthesis of aromatic amino acids (AroAAs). In most methanogens, pentoses are produced by the oxidative pentose pathway via oxidative decarboxylation of hexoses (Choquet *et al.*, 1994). It was proposed that *M. maripaludis* makes pentoses by a nonoxidative pentose phosphate (NOPP) pathway (Figure 6.10; Yu *et al.*, 1994). Some studies of several organisms confirmed certain aspects of the proposed pathway, whereas others provided the evidence in contrast to the formation of AroAAs by E4P through the NOPP pathway. The alternative explanation of the results has been studied—that E4P may not be a precursor of AroAA biosynthesis. A study was carried to determine the labeling patterns by NMR of ribose in cells of *M. maripaludis* grown on  $[2-^{13}\text{C}]\text{acetate}$  since isotope enrichment of ribose is expected to be affected by the removal of E4P for AroAA biosynthesis. Because a quantitative measurement of the enrichment ratio depends on the accuracy of signal integrations, the  $^1\text{H}$  and  $^{13}\text{C}$  were recorded with sufficiently long relaxation delays, which were 10 s for  $^1\text{H}$  and 20 s for  $^{13}\text{C}$ , and decoupling for either  $^1\text{H}$  or  $^{13}\text{C}$  was not used to avoid NOE effects on the observed signal intensities.

The study found that the extent of  $^{13}\text{C}$  enrichment at the  $\text{C}'_1$  of cytidine and uridine was not consistent with the proposed NOPP pathway, which should yield 50% of labeled  $\text{C}'_1$  derived from the  $^{13}\text{C}_2$  of acetate. The enrichment determined by the  $^1\text{H}$  NMR was 66.6% at the  $\text{C}'_1$  of cytidine (Figure 6.11a,  $^1\text{H}$  spectra of  $^{13}\text{C}$ -labeled cytidine and uridine from the biosynthesis of *M. maripaludis* cells grown on  $[2-^{13}\text{C}]\text{acetate}$ ). Furthermore, no label at  $\text{C}'_2$ ,  $\text{C}'_3$ ,  $\text{C}'_4$ , and

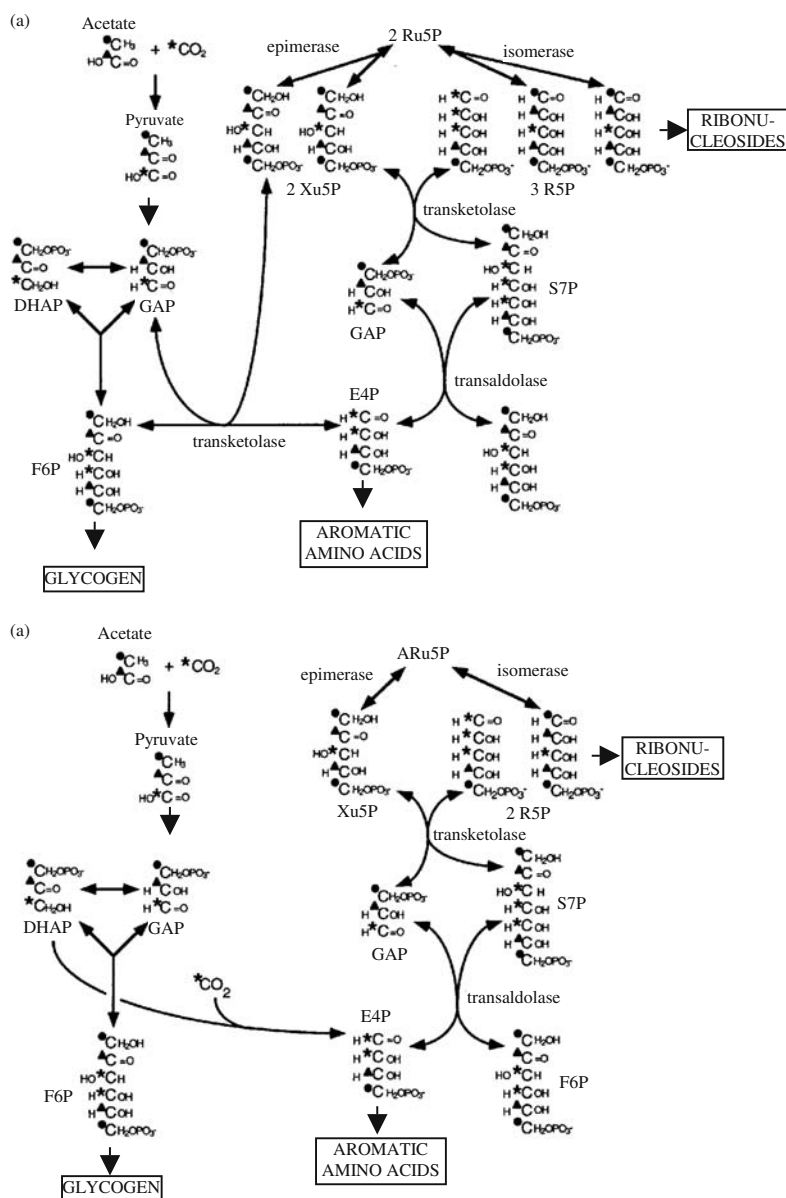


**Figure 6.10.** The NOPP pathway in methanococci. Thicker arrows indicate multiple steps. DHAP, dihydroxyacetone phosphate; GAP, glyceraldehyde 3-phosphate; F6P, fructose-6-phosphate; Xu5P, xylulose 5-phosphate; Ru5P, ribulose 5-phosphate; R5P, ribose 5-phosphate; S7P, sedoheptulose 7-phosphate.  $^{13}\text{C}$ -label sources: ●, C<sub>2</sub> of acetate; ▲, C<sub>1</sub> of acetate; \*, CO<sub>2</sub>. (a) The pathway and expected labeling patterns (Yu *et al.*, 1994). Consumption of E4P for AroAA biosynthesis increases the amount of R5P formed via Xu5P. (b) Modified pathway as proposed by Choquet *et al.* (1994). E4P is formed by carboxylation of a triose such as DHAP, and the F6P-dependent transketolase reaction is absent. Although the labeling pattern of E4P is unchanged, 50% of the R5P is now formed via Xu5P, and the labeling pattern of ribose is not affected by the consumption of E4P for AroAA biosynthesis (reproduced with permission from Tumbula *et al.*, *J. Bacteriol.* 179, 6010, 1997. Copyright © 1997 American Association for Microbiology).

C<sub>6</sub> of cytidine was detected, indicating that scrambling of the isotope did not occur (Wood and Katz, 1958). Because of signal overlapping, the extent of <sup>13</sup>C enrichment of uridine was determined using the resolved signal of <sup>1</sup>H attached to un-enriched <sup>12</sup>C<sub>5</sub> and was based on the assumption that both <sup>1</sup>H spins attached to C'<sub>1</sub> and to C<sub>5</sub> contribute equally to the total integrals of observed signals. The enrichment at C'<sub>1</sub> of uridine was observed as 66.3%, which is about the same level as in cytidine. The <sup>13</sup>C spectra of the two compounds provided the same results: that the amount of <sup>13</sup>C<sub>1</sub> carbons, obtained from C<sub>2</sub> of acetate, in both compounds is  $\frac{2}{3}$  of the total C'<sub>1</sub> carbons.

The NMR results (Figure 6.11) were interpreted as follows. According to the NOPP pathway (Figure 6.10), 66.7% or more of the C<sub>1</sub> of ribose will come from the C<sub>2</sub> of acetate because exactly  $\frac{2}{3}$  of the C<sub>1</sub> of ribose will be obtained from the C<sub>2</sub> of acetate if E4P is not diverted from the pathway or the fraction will be increased if E4P is removed from the pathway

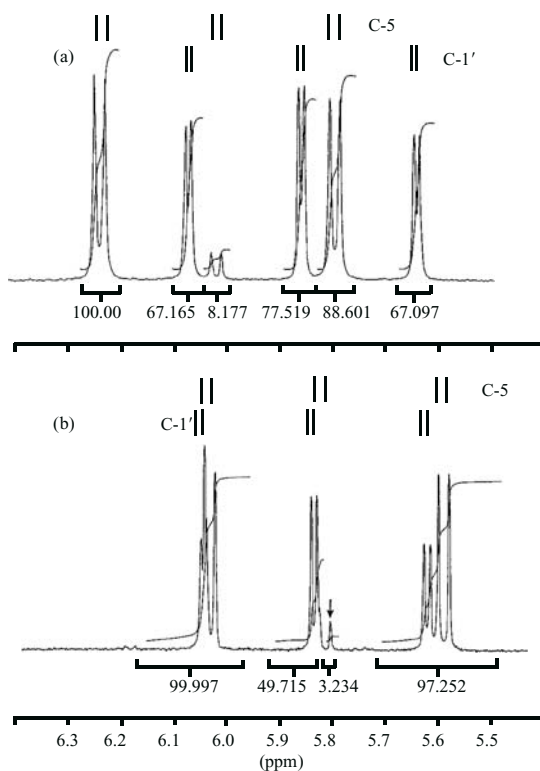


**Figure 6.11.** Proton NMR spectra for protons at C'<sub>1</sub> and C<sub>5</sub> of cytidine and uridine from *M. maripaludis* following growth on [2-<sup>13</sup>C]acetate. The integrals of the peaks are given below the spectra. (a) Cytidine. The <sup>1</sup>J<sub>CH</sub> coupling constants for the C'<sub>1</sub> and C<sub>5</sub> protons were 168 and 172 Hz, respectively. For calculation of the enrichment of cytidine: C'<sub>1</sub>% = (67.165 + 67.097)/(67.165 + 67.097 + 77.519) = 63.8%, C<sub>5</sub>% = (88.6 + 100)/(88.6 + 100 + 8.17) = 95.8%. (b) Uridine. The <sup>1</sup>J<sub>CH</sub> coupling constants for the C'<sub>1</sub> and C<sub>5</sub> protons were 170 and 176 Hz, respectively. The arrow indicates one of the <sup>12</sup>C peaks for C<sub>5</sub>, whereas the other <sup>12</sup>C peak overlaps the <sup>12</sup>C peaks for C'<sub>1</sub>. For calculation of the <sup>13</sup>C enrichment, it was assumed that the total signal (99.997 + 49.715 + 3.234 + 97.252 = 250.198) could be divided equally between C'<sub>1</sub> and C<sub>5</sub>. The <sup>13</sup>C enrichment of C<sub>5</sub> was calculated as [125.099 - (3.234 × 2)]/125.099 = 94.8%. The <sup>13</sup>C enrichment of C'<sub>1</sub>, uncorrected for the maximal enrichment, was calculated as: (125.099 - 49.715 + 3.234)/125.099 = 62.8% (reproduced with permission from Tumbula *et al.*, *J. Bacteriol.* 179, 6010, 1997. Copyright © 1997 American Association for Microbiology).



for AroAA biosynthesis. Since the molar ratio of AroAA to ribose is  $c.1:2$  (Neidhardt and Umbarger, 1996), 83% of ribose will be produced from the  $C_2$  of acetate if E4P is used for AroAA biosynthesis. Based on the NMR results and the fact that the genes for the first two enzymes in the common AroAA pathway were not identified in the genome, the conclusion was reached that only the NOPP pathway is used for E4P biosynthesis and E4P is not used for AroAA biosynthesis.

Another example is the study of insulin regulation by the muscle glycogen synthesis pathway (Shulman *et al.*, 1990; Taylor *et al.*, 1992; Gruetter *et al.*, 1994). Malfunction of this regulation leads to insulin-independent (type II) diabetes. The disease is believed to have a strong genetic component in addition to being related to environmental factors, such as diet and exercise. Although it was known that the increase of glucose levels in patients after a meal is due to metabolic pathways in muscle and/or the liver not responding properly to the insulin, it was not clear which metabolic pathway dominates the insulin resistance. One-dimensional  $^{13}\text{C}$  NMR was used to study the insulin stimulated glycogen synthesis. Insulin and  $^{13}\text{C}$ -labeled glucose were infused into healthy adults and patients to create post-meal conditions. The  $^{13}\text{C}$  signal of  $^{13}\text{C}$ -labeled glucose was measured at different times during the infusion to monitor the flow of glucose into muscle glycogen as a function of time. The muscle glycogen is increased as shown by the increase of the  $^{13}\text{C}$  signal with time (Figure 6.12). In the  $^{13}\text{C}$  spectra, the resonance frequency of the  $^{13}\text{C}$  spins in glycogen obtained from the glucose is well-resolved from the signals of  $^{13}\text{C}$ -labeled glucose and other metabolites in the muscle. The rate of muscle glycogen synthesis in the patients is two-fold slower than that obtained from the healthy group (Figure 6.13), which quantitatively explains the patients' lower insulin-stimulated glucose uptake. Therefore, insulin-stimulated glycogen synthesis in muscle is the major metabolic pathway for consuming excess glucose in healthy adults. A defect in muscle glycogen synthesis is a major cause for the decreased insulin sensitivity in the insulin-independent diabetes patients.

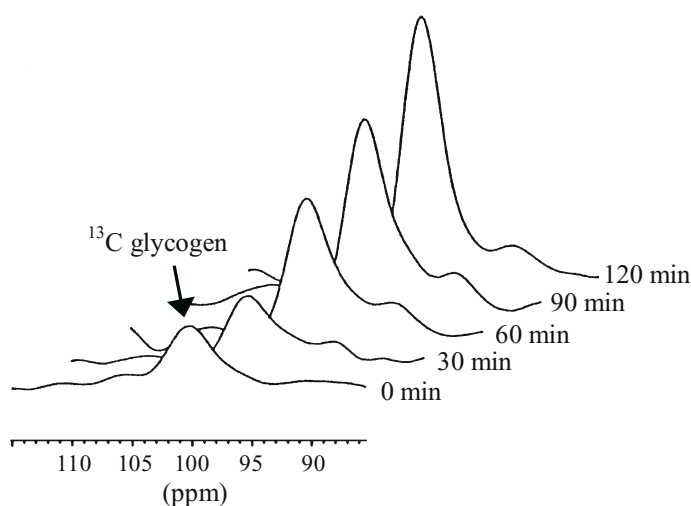


**Figure 6.12.**  $^{13}\text{C}$  spectra of muscle glycogen as a function of time. The samples were obtained at different times from healthy subjects during an infusion of insulin and  $^{13}\text{C}$ -labeled glucose. The resonance frequency of the  $^{13}\text{C}$  isotope in the glycogen molecule was resolved from background signals of  $^{13}\text{C}$ -labeled glucose and other biological metabolites in the muscle (reproduced with permission from Shulman *et al.*, *N. Engl. J. Med.* 322, 223, 1990. Copyright © 1990 Massachusetts Medical Society).

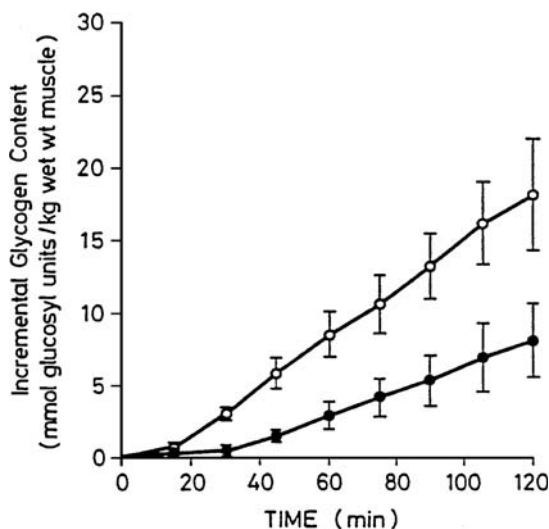


**Figure 6.13.** Muscle glycogen concentration calculated from the  $^{13}\text{C}$  NMR spectra during an insulin and glucose infusion for patients and healthy controls. The diabetics (closed symbols) synthesize glycogen more slowly than control subjects (open symbols). Quantitative features of this study showed that insulin-stimulated muscle glycogen synthesis is the major metabolic pathway of glucose disposal in both groups, and that impairments in this pathway are responsible for the chronic hyperglycemia in patients (reproduced with permission from Shulman *et al.*, *N. Engl. J. Med.* 322, 223, 1990. Copyright © 1990 Massachusetts Medical Society).

## QUESTIONS

- 6.1. What is the maximum concentration of ligand, compared to the concentration of protein, used in the diffusion method in the study of ligand–protein binding? And explain why.
- 6.2. What is the primary principle underlying the SAR-by-NMR method? And why can NMR be used for that purpose?
- 6.3. If compound A has a dissociation constant  $K_D$  of  $2 \times 10^{-3}$  M and compound B has a  $K_D$  of  $2 \times 10^{-6}$  M, which are binding to two different sites of a protein, what is the dissociation constant  $K_D$  likely for compound C that is made from the structurally linked A and B? And explain why.
- 6.4. Both transfer NOE and saturation transfer difference (STD) experiments make use of dipolar cross-relaxation to determine the binding complex of ligand to protein. What are the differences between these two methods? And what are the advantages and limitations of the two?
- 6.5. If a free ligand has a diffusion constant eight times larger than that of the protein, what is the ratio of the intensities of peaks from the free ligand to those from bound ligand likely to be when using the same parameters (gradient strength, delays, etc.) in the gradient diffusion measurements for the samples with and without protein?

- 6.6. From a series of  $^1\text{H}$  diffusion experiments, the slope from the plot fitting of  $\ln(I/I_0)$  vs  $G^2$  is 28.68. The gradient duration of 5 ms and diffusion time  $\Delta$  of 300 ms were used for all experiments. What is the determined diffusion constant for the solute?
- 6.7. Why can STD experiments only be used for studying large proteins? What would happen if the method is used for smaller proteins?
- 6.8. In addition to a library of compounds, what kind of NMR sample do you need to use the SAR-by-NMR method to screen the binding affinity of ligand to a protein?

## REFERENCES

- Breeze, A., *Prog. Nucl. Magn. Reson. Spectrosc.* **36**, 323 (2000).
- Cheng, Y.-C. and W.H. Prusoff, *Biochem. Pharmacol.* **22**, 3099 (1973).
- Choquet, C.G., J.C. Richards, G.B. Patel, and G.D. Sprott, *Arch. Microbiol.* **161**, 481 (1994).
- Clore, G.M. and A.M. Gronenborn, *J. Magn. Reson.* **48**, 402 (1982).
- Dalvit, C. and J.M. Böhlen, *NMR Biomed.* **10**, 285 (1997).
- Fesik, S.W., R.T. Gampe Jr., T.F. Holzman, D.A. Egan, R. Edalji, J.R. Luly *et al.*, *Science* **250**, 1406 (1990).
- Gahmberg, C.G., *Curr. Opin. Cell Biol.* **9**, 643 (1997).
- Gemmecker, G., E.T. Olejniczak, and S. Fesik, *J. Magn. Reson.* **96**, 199 (1992).
- Gruetter, R., I. Magnusson, D.L. Rothman, R.G. Shulman, and G.I. Shulman, *Magn. Reson. Med.* **31**, 583 (1994).
- Hajduk, P.J., G. Steppard, D.G. Nettesheim, E.T. Olejniczak, S.B. Shuker, R.P. Meadows *et al.*, *J. Am. Chem. Soc.* **119**, 5818 (1997a).
- Hajduk, P.J., J. Dinges, G.F. Miknis, M. Merlock, T. Middleton, D.J. Kempf *et al.*, *J. Med. Chem.* **40**, 3144 (1997b).
- Johnson Jr., C.S., *Prog. Nucl. Magn. Reson. Spectrosc.* **34**, 203 (1999).
- Klein, J., R. Meinecke, Mayer, M., and B. Meyer, *J. Am. Chem. Soc.* **121**, 5336 (1999).
- Liu, G., J.R. Huth, E.T. Olejniczak, R. Mendoza, P. DeVries, S. Leitza *et al.*, *J. Med. Chem.* **44**, 1202 (2001).
- Liu, G., J.T. Link, Z. Pei, E.B. Reilly, S. Leitza, B. Ngygen *et al.*, *J. Med. Chem.* **43**, 4025 (2000).
- Mayer, M. and B. Meyer, *Angew. Chem., Int. Ed.* **38**, 1784 (1999).
- Mayer, M. and B. Meyer, *J. Am. Chem. Soc.* **123**, 6108 (2001).
- Meyer, B., T. Weimar, and T. Peters, *Eur. J. Biochem.* **246**, 705 (1997).
- Neidhardt, F.C. and H.E. Umbarger, in F.C. Neidhardt, R. Curtiss III, J.L. Ingraham, E.C.C. Lin, K.B. Low, B. Magasanik *et al.* (ed.), “*Escherichia coli* and *Salmonella*: cellular and molecular biology,” 2nd edn, American Society for Microbiology, Washington, DC, p. 13 (1996).
- Ni, F., *Prog. Nucl. Magn. Reson. Spectrosc.* **26**, 517 (1994).
- Price, W.S. and P.W. Kuchel, *J. Magn. Reson.* **94**, 133 (1991).
- Shuker, S.B., P.J. Hajduk, R.P. Meadows, and S.W. Fesik, *Science* **274**, 1531 (1996).
- Shulman, G.I., D.L. Rothman, T. Jue, P. Stein, R.A. DeFronzo, and R.G. Shulman, *N. Engl. J. Med.* **322**, 223 (1990).
- Sligh, J.E., C.M. Ballantyne, S.S. Rich, H.K. Hawkins, C.W. Smith, A. Bradley *et al.*, *Proc. Natl. Acad. Sci., USA* **90**, 8529 (1993).
- Stejskal, E.O. and J.E. Tanner, *J. Chem. Phys.* **42**, 288 (1965).

- Stilbs, P., *Prog. Nucl. Magn. Reson. Spectrosc.* **19**, 1 (1987).
- Taylor, R., T.B. Price, D.L. Rothman, R.G. Shulman, and G.I. Shulman, *Magn. Reson. Med.* **27**, 13 (1992).
- Tumbula, D.L., Q. Teng, M.G. Bartlett, and W.B. Whitman, *J. Bacteriol.* **179**, 6010 (1997).
- Wood, H.G. and J. Katz, *J. Biol. Chem.* **233**, 1279 (1958).
- Yu, J.-P., J. Ladapo, and W.B. Whitman, *J. Bacteriol.* **176**, 325 (1994).
- Zwahlen, C., P. Legault, S.J.F. Vincent, J. Greenblatt, R. Konrat, and L.E. Kay, *J. Am. Chem. Soc.* **119**, 711 (1997).